Applied Catalysis B: Environmental 111–112 (2012) 376–380

Contents lists available at SciVerse ScienceDirect

Applied Catalysis B: Environmental

journal homepage: www.elsevier.com/locate/apcatb

Electrochemical activity of ruthenium and iridium based catalysts for oxygen evolution reaction

N. Mamaca [a], E. Mayousse [b], S. Arrii-Clacens [a], T.W. Napporn [a], K. Servat [a], N. Guillet [b], K.B. Kokoh [a,*]

[a] "Equipe E-lyse" LACCO UMR CNRS 6503, Université de Poitiers, Département de Chimie, 4 rue Michel Brunet – B27, BP 633, 86022 Poitiers Cedex, France
[b] CEA, LITEN, DEHT/LCPEM, 17 rue des Martyrs, F-38054 Grenoble, France

ARTICLE INFO

Article history:
Received 13 July 2011
Received in revised form 6 October 2011
Accepted 11 October 2011
Available online 18 October 2011

Keywords:
Water electrolysis
Iridium
Ruthenium based electrocatalysts
Metal oxides
Pechini–Adams

ABSTRACT

Powders of ruthenium and iridium-based materials were synthesized by the thermal decomposition process. The suitable heat treatment of the polymeric precursors allowed to recover metal oxides free from organic carbon, which can be oxidized to carbon dioxide during H_2O splitting at elevated potentials. The materials were examined by various physicochemical techniques in order to understand their electrochemical behavior as anodes in a 5 cm^2 single proton exchange membrane water electrolyzer. Although the presence of Ir in the electrocatalyst composition contributes undoubtedly to its stability against ruthenium dissolution and the Faradaic efficiency of the PEM electrolysis cell, its great amount increases the overpotential value. The activity of the home made $Ru_xIr_{1-x}O_2$ anodes towards the oxygen evolution reaction occurs at *ca.* 1.5 V at 25 °C.

1. Introduction

The massive utilization of fossil fuels is contributing more and more to a greenhouse effect mainly due to industrial processes and waste combustion [1]. The present environmental constraints require the development of clean and efficient energy carriers free from carbon such as hydrogen [2–5]. Water electrolysis in a proton exchange membrane cell is one of the possibilities to obtain hydrogen by an environmentally friendly way [6–14]. This procedure has the advantage to produce simultaneously hydrogen and oxygen without by-product. The Pechini–Adams method which consists in preparing materials by thermal decomposition of polymeric metal precursors is very proven for the preparation of anode catalysts for Direct Alcohol Fuel Cells (DAFCs) [15–20] and DSA-type electrodes (Dimensionally Stable Anode) [21–25]. Although it exists an analogy between Proton Exchange Membrane (PEM) Fuel Cell and PEM water electrolyzer, the main difference remains in the activation of the water molecule at the anode in an electrolysis cell. Indeed, if platinum constitutes the reference as electrocatalyst for producing hydrogen without overpotential, the splitting of H_2O to O_2 occurs at its surface at high potentials, compared to those established thermodynamically [14]. Conversely, it makes of Pt a material less effective and attractive than ruthenium and iridium as catalysts for Oxygen Evolution Reaction (OER) and only few oxides electrode materials can withstand strongly oxidative conditions in acidic environments. They are restricted essentially to RuO_2, IrO_2 and MnO_2 [22–32]. Many studies have shown that Ru is the more efficient metal for H_2O splitting. Unfortunately, though its oxide at an oxidation state IV is considered as the more active catalyst to split water at potentials close to the thermoneutral one (1.48 V at 298 K), it evolves very fast towards an unstable form (RuO_4) and subsequently to its dissolution [33,34]. However, to improve its stability and corrosion resistance, several authors suggested its "dilution" with IrO_2 without decreasing the activity of the anode for OER [6,35,36].

The aim of this work is to report results on the development of ternary $Ru_xIr_{1-x}O_2$ electrocatalysts prepared by thermal decomposition of a polymeric precursor and their application in the oxygen evolution reaction. Several investigations in PEMFC have revealed that the dilution and the dispersion of the catalyst in carbon powder enabled to reduce the amount of costly precious metals [16,17,37]. But in the case of the water electrolysis, the potential applied to the anode ranges between 1.3 and 2 V *vs.* SHE. The presence of carbon in the active layer definitely leads to the oxidation of the supporting substrate with the following reaction [38,39]:

$$C + 2H_2O \rightarrow CO_2 + 4H^+ + 4e^- \text{ at } 0.206\,V \textit{ vs } .SHE. \quad (1)$$

Consequently, the catalysts prepared in the present work would not be supported on a carbon powder as usually done in PEM fuel cell devices. Moreover, to decrease the overpotential and to stabilize the anode catalyst, different Ir contents were added in the composition of ruthenium based electrodes.

* Corresponding author. Tel.: +33 549 45 41 20; fax: +33 549 45 35 80.
E-mail address: boniface.kokoh@univ-poitiers.fr (K.B. Kokoh).

0926-3373/$ – see front matter © 2011 Elsevier B.V. All rights reserved.
doi:10.1016/j.apcatb.2011.10.020

2. Experimental

2.1. Catalyst preparation

Electrocatalysts were synthesized by thermal decomposition of polymeric precursors well-known as the Pechini–Adams method [40]. The Ru and Ir polymeric precursors (metal–resin) were separately prepared, mixing citric acid (CA) (Sigma Aldrich) in ethylene glycol (EG) (Sigma Aldrich) at 60–65 °C. The precursor salt $RuCl_3{\cdot}xH_2O$ (Sigma–Aldrich) was dissolved in an acidic solution (HCl/H_2O 1:1, v/v) then it was added slowly at a molar ratio of 1:4:16 of CA/EG/metal. After total dissolution of the precursor salt, the temperature was raised to 90 °C and kept at this level for 2–3 h, under vigorous stirring. In a similar way iridium was prepared with the same ratio from $IrCl_3{\cdot}xH_2O$. Then different composition of ruthenium and iridium were prepared and calcined until 400 °C in oven under oxygen atmosphere in order to obtain oxide species. The temperature was firstly increased to 250 °C at a rate of 1 °C min^{-1} and it was kept there for 1 h. Then, the temperature was increased to 350 °C at a rate of 10 °C min^{-1}, and kept for another 1 h. Afterwards, the temperature was increased up to 400 °C at a rate of 30 °C min^{-1} and kept there for 1 h to recover a material free from organic carbon.

2.2. Preparation of ink

The obtained catalytic powders were used to prepare the different catalytic anodes. The powder (4 mg) was dispersed in a solution (839 μL) containing water (725 μL) and a Nafion® solution (114 μL) (5 wt.% in aliphatic alcohol, Aldrich). The resulting ink was ultrasonically homogenized for few hours. For each electrochemical experiment 15 μL of the ink was deposited onto a gold disk of 5 mm diameter which was previously polished with alumina (0.5 μm) to a mirror-finish to serve as supporting substrate of the working electrode; the catalytic ink was then dried under nitrogen (U quality, from l'Air Liquide).

2.3. Physicochemical characterizations

The catalysts were characterized by electrochemical and physical methods. The surface morphology, microstructure and elemental composition of the deposited oxide catalyst were analyzed by transmission electron microscopy (TEM) and high resolution transmission electron microscopy (HRTEM) on a JEOL/JEM 2100 UHR, equipped with an EDX detector Si-Li JEOL which permits energy dispersive X-ray absorption analyses. The structure of the synthesized materials was examined by X-ray diffraction (XRD) on a Bruker AXS D8 Advance Bragg–Brentano diffractometer operated with a copper tube ($\lambda = 0.15406$ nm) powered at 30 kV and 30 mA. This apparatus is equipped with a Position Sensitive Detector (PSD), VANTEC-1, including K_β filter and working in scanning mode. Powder samples were deposited on a silicium wafer (911) after crushing and sifting, and measurements were carried out in the 2θ range 20–90° with a step size of 0.049° and a time per step of 10 s. Brunauer–Emmett–Teller (BET) analyses were realized with ASAP 2010 micromeritics using N_2 as adsorption gas at liquid N_2 temperature (77 K).

2.4. Electrochemical measurements

All the solutions used in this work were prepared with 18.2 MΩ cm water produced at 20 °C and purified by a Millipore-Milli-Q system. Electrochemical studies were performed using 0.5 mol L^{-1} H_2SO_4 (Merck) as supporting electrolyte.

The electrochemical measurements (voltammetry, chronoamperometry and chronopotentiometry) were performed in a conventional three-electrode electrochemical glass cell (20 mL) using Radiometer Analytical (PGZ 402) potentiostat Electrochemical Interface. A Reversible Hydrogen Electrode (RHE) and a glassy carbon plate (8 cm^2) electrically connected with a gold wire served as reference and counter electrodes, respectively. The working electrode was composed of the catalytic ink made from the suitable mixture of a $Ru_xIr_{1-x}O_2$ powder, a Nafion® 5 wt.% solution and water. This catalytic ink was then deposited at the surface of a gold substrate as conductive carrier (0.38 mg cm^{-2}).

Table 1
Anode and cathode catalysts loadings used for the membrane electrode assemblies.

Anode	Membrane	Cathode
$Ru_{70}Ir_{30}O_2$ 10 wt.% Nafion, 1.68 mg cm^{-2}	N115	Pt/C (46.1 wt.%) 27 wt.% Nafion – 0.2 mg_{Pt} cm^{-2}
$Ru_{80}Ir_{20}O_2$ 10 wt.% Nafion, 1.56 mg cm^{-2}	N115	Pt/C (46.1 wt.%) 27 wt.% Nafion – 0.36 mg_{Pt} cm^{-2}
IrO_2 from Sigma 10 wt.% Nafion, 2.34 mg cm^{-2}	N115	Pt/C (46.1 wt.%) 27 wt.% Nafion – 0.56 mg_{Pt} cm^{-2}

2.5. Preparation of the catalysts and of the membrane electrode assemblies (MEAs)

The membrane electrode assemblies (MEAs) were prepared by the decal method. The $Ru_xIr_{1-x}O_2$ catalyst ink containing 10 wt.% Nafion® from a dispersion in aliphatic alcohol (D-520, 5 wt.%, DuPont) was sprayed on a PTFE substrate. This hot pressing method makes easier the transfer of the catalytic layers and enables to reach a catalyst loading of about 2.5 mg cm^{-2} for binary Ru–Ir materials and 2.34 mg cm^{-2} for IrO_2. Conversely to the anode catalysts which do not contain carbon powder as supporting substrate, the cathode catalyst can be carbon supported materials. Because hydrogen evolution reaction occurs without overpotential, Pt/C electrodes were herein used as cathode electrocatalysts. They were prepared by roll coating an ink made of Pt/C powder (TEC10V50E, 46.1 wt.%, Tanaka), 27 wt.% of Nafion® (D-520, 5 wt.%, DuPont) and deionised water, on a PTFE substrate. The aimed Pt loading was of 0.4 mg cm^{-2}. Samples of the both electrodes were punched (26 mm diameter) to give 5.31 cm^2 PTFE supported electrodes. These samples were carefully weighted then hot pressed on each side of a pretreated Nafion® NRE 115 CS membrane at 135 °C at a pressure of 4 MPa. PTFE support was removed and weighted to calculate the real amount of catalyst deposited on the membrane (Table 1). Performances were determined in a single electrolyzer cell with an electrode geometric surface area of 5 cm^2. A titanium sintered disc acts as anodic current collector while a carbon gas diffusion layer (SGL 34BC) was used at the cathodic side. Tests were performed at room temperature and atmospheric pressure.

3. Results and discussion

3.1. Physicochemical characterization of the materials

The heat treatment of the resins issued from the polymeric metallic precursors consists in obtaining catalytic materials free from organic carbon species to avoid occurrence of CO_2 formation (cf. Eq. (1)) during the anodic activation of H_2O at high potentials. Therefore, TEM measurements were performed to analyze the morphology of synthesized particles. Fig. 1 reveals images in which the heterogeneous particles size varies from 1.5 to 70 nm (Table 2). Although agglomerate size may influence the properties of the Membrane–Electrode-Assembly (MEA) layer [22], it could be considered that in the absence of carbon substrate as a catalyst support, the material powders obtained are similar in morphology to

Table 2
Specific surface areas and particle diameters of Ru and Ir based catalysts.

Sample	Particle diameter by TEM (nm)	Particle diameter by XRD (nm)	BET surface area ($m^2\ g^{-1}$)
RuO_2	6–10	10	26.28
$Ru_{0.8}Ir_{0.2}O_2$	7–70	20–60	44.97
$Ru_{0.7}Ir_{0.3}O_2$	6–50	20–50	76.92
IrO_2	1.5–20	7–27	6.12

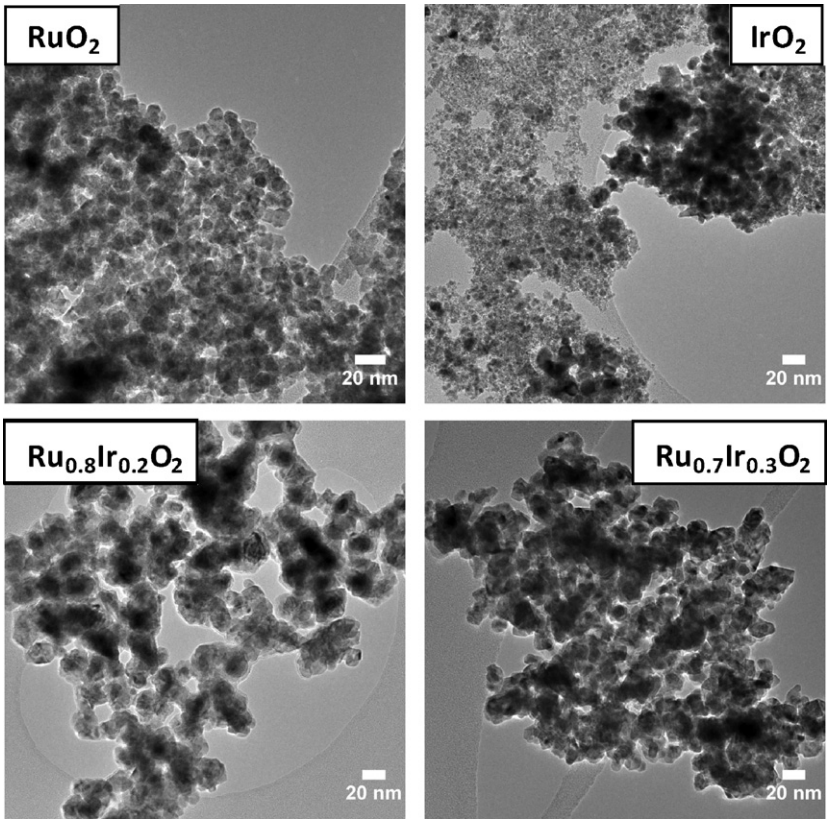

Fig. 1. TEM images of Ru and Ir based catalysts prepared by the thermal decomposition process.

those reported in the literature and prepared under the same conditions with the same Pechini–Adams method [20,21,41]. Based on the fact that IrO_2 improves the oxidation resistance of RuO_2 which is the best metallic oxide in the H_2O splitting, the $Ru_xIr_{1-x}O_2$ materials were analyzed by EDX, which well shows the presence of both Ru and Ir oxides in the catalyst composition. Importantly, the average experimental composition of the $Ru_{0.8}Ir_{0.2}O_2$ catalyst is similar to the nominal one, while that of $Ru_{0.7}Ir_{0.3}O_2$ becomes close to $Ru_{0.77}Ir_{0.23}O_2$ after the heat treatment process at 400 °C. This difference in composition could probably be due to either a metal loss during the heat treatment or to the delicate sampling of each colloid for constituting the nominal mixture. This last result is confirmed by XRD pattern which shows an average composition close to $Ru_{0.82}Ir_{0.18}O_2$.

The eletrocatalytic properties and chemical stabilities of the active oxides can be tuned by changing their surface compositions and physical structures. XRD patterns for the bimetallic powders were compared with the monometallic ones prepared under the same operating conditions (Fig. 2). In the case of Ru sample, XRD pattern reveals the presence of oxide in hexagonal structure whereas it reveals, for Ir sample, the presence of metal and oxide phase, respectively in cubic and tetragonal structure, as for the bimetallic systems where metallic and oxide forms coexist. The broad peaks centered at *ca.* 28° and 58° correspond to the (1 1 0) and (2 2 0) reflections of RuO_2. The presence of IrO_2 was also confirmed by the main peaks centered at *ca.* 28, 35 and 40°, which represent the (1 1 1), (1 0 1) and (1 1 1) reflections, respectively. Although the metallic forms of Ru and Ir are present, experimental lattice parameters for the different systems were calculated to know whether

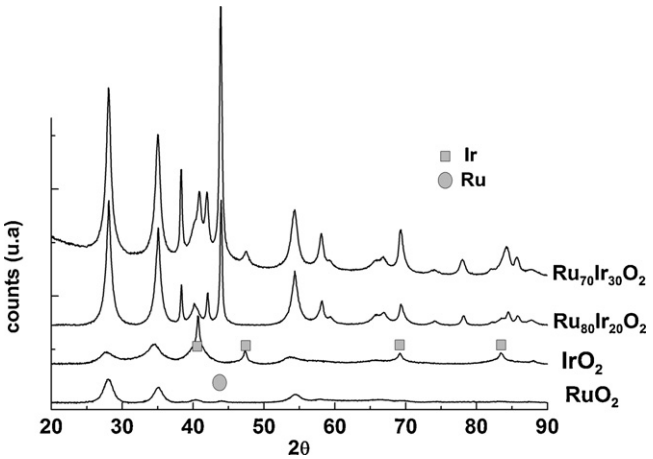

Fig. 2. X-ray diffraction patterns of Ru and Ir based catalysts prepared by the thermal decomposition process.

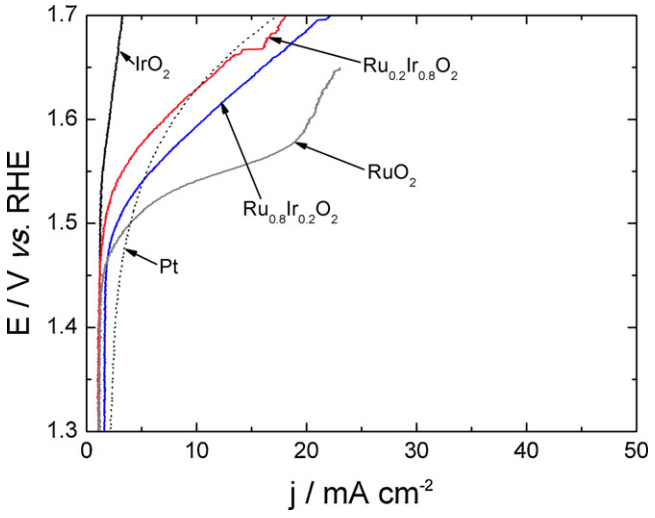

Fig. 3. *I–E* polarization curves at 5 mV s^{-1} in 0.5 M H_2SO_4 as function of the nature of the anode electrode material.

the RuO_2 and IrO_2 materials with intense peaks would coexist in the form of (Ru, Ir)O_2 solid solution in the prepared materials [36,42,43]. The results show that we do not have alloy because of a small change. Thanks to Scherrer formula, the average particles size could be estimated and compared to the TEM value (Table 2). The difference would come from the fact that XRD permit only to make an estimation of the crystallized domain size.

The specific surface areas of the catalysts were evaluated by performing Brunauer–Emmett–Teller (BET) measurements (Table 2). It seems that lower specific surfaces are obtained than those which could be expected. This could be explained by a difference in kinetics of metals reduction during the heat treatment as function of porosity of the material. This kinetics process may involve a well-dispersion of a metal which uses the second one as supporting substrate. As a result, the considered bimetallic catalysts give larger values that those estimated with RuO_2 and IrO_2. Indeed, the specific surface area increases with the Ir content in the $Ru_xIr_{1-x}O_2$ material.

3.2. Electrochemical characterization of the catalysts

Preliminary investigations were performed on the synthesized catalysts for lying around their electrochemical behavior in an acidic supporting electrolyte (0.5 M H_2SO_4). As can be seen the polarization curves in Fig. 3, the catalyst RuO_2 presents the best onset potential towards the activation of water in comparison with IrO_2 and Pt. Furthermore, it is well-known that the Ir content in the Ru-based catalyst composition contributes to its stability against dissolution without increasing overpotential at its surface.

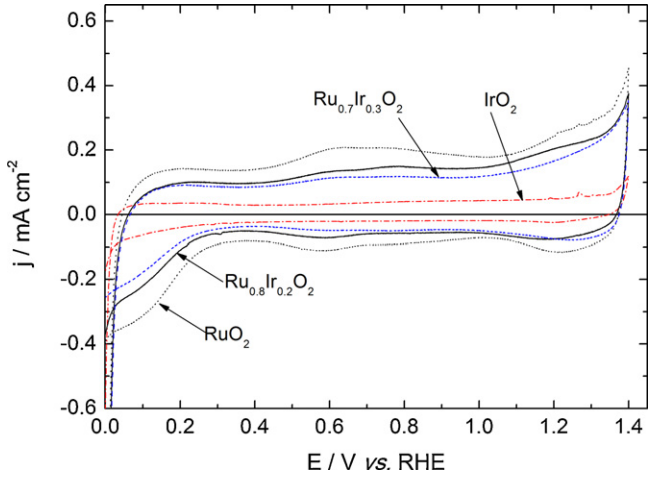

Fig. 4. Cyclic voltammograms of Ru and Ir based electrodes in a 0.5 mol L^{-1} H_2SO_4 solution at room temperature (25 °C) (scan rate = 20 mV s^{-1}).

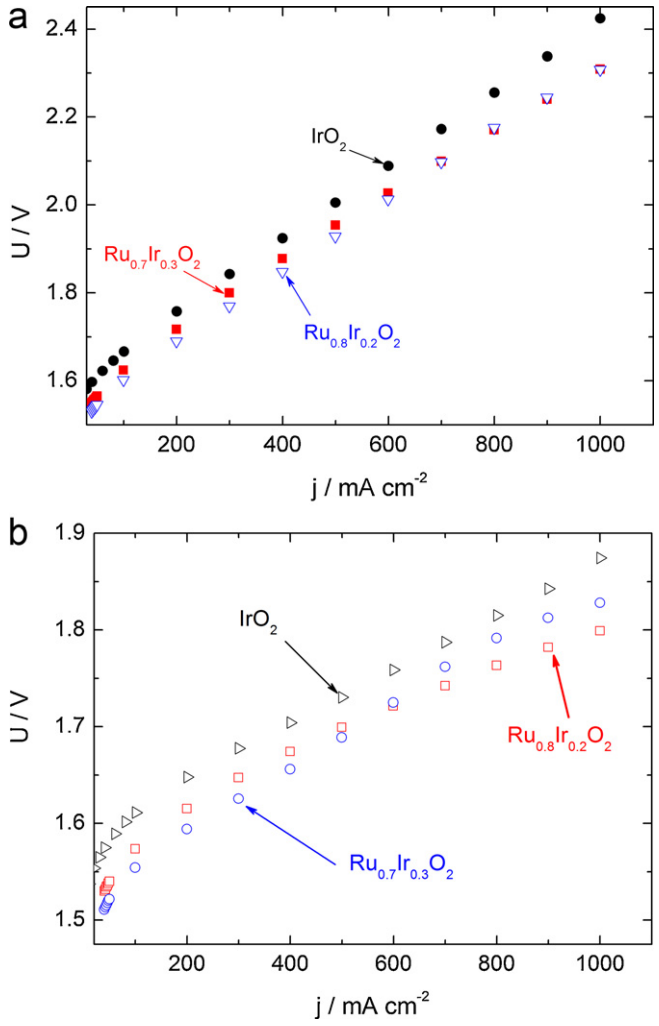

Fig. 5. Electrical performances of a 5 cm^2 PEM electrolyzer at room temperature and atmospheric pressure using IrO_2 and $Ru_xIr_{1-x}O_2$ anodes (2.5 mg cm^{-2} catalyst loading) and Nafion® 115 membrane. (a) IrO_2 (●), $Ru_{0.8}Ir_{0.2}O_2$ (▽) and $Ru_{0.7}Ir_{0.3}O_2$ (■) without ohmic resistance correction. (b) IrO_2 (▷), $Ru_{0.8}Ir_{0.2}O_2$ (□) and $Ru_{0.7}Ir_{0.3}O_2$ (○) with ohmic resistance correction.

The cyclic voltammogram of each Ru-based electrode was recorded to evaluate its behavior in supporting electrolyte (Fig. 4). There is shrinkage of the voltammogram when decreasing the Ir content in the catalyst composition.

Capacitance values (C_s) of the electrode materials are estimated from the respective voltammograms, as follows:

$$C_s = \frac{I}{v \times m} \quad (2)$$

where I is the current intensity, v is the scan rate and m, the catalyst weight deposited onto the substrate. The values obtained are averaged by measuring the current at every 100 mV from 0.3 to 0.7 V *vs.* RHE. 9.4 and 11.4 F g^{-1} were obtained for the bimetallic electrocatalysts $Ru_{0.7}Ir_{0.3}O_2$ and $Ru_{0.8}Ir_{0.2}O_2$ respectively, while 3.6 and 17 F g^{-1} are estimated for IrO_2 and RuO_2, respectively. These results confirm those reported in literature where it was shown

that the capacitance of the electrode–electrolyte interface decrease with the Ir content in the bimetallic composition [35].

3.3. Performance of electrolysis cell

The membrane electrodes assembly (MEA) was made with a Pt/C cathode and the home made $Ru_xIr_{1-x}O_2$ materials as anodes (approximately 2.5 mg cm^{-2}). Fig. 5 shows the performances of a 5 cm^2 single Proton Exchange Membrane (PEM) cell which operates at room temperature (25 °C). Although any measurement was not performed in the electrolyzer cell with RuO_2 anode, the results were found at lower overpotentials with Ru–Ir binary materials than those obtained with commercial IrO_2 (from Sigma). Any comparison with literature is difficult since the reported performances were measured at higher temperatures than those obtained herein. However, they are in good agreement with those of several works where bimetallic anodes are more active than IrO_2 [6,8,9,27,44].

As can be seen in Fig. 5, H_2O splitting occurs at *ca.* 1.5 V at the Ru–Ir binary catalysts, which is very close to the thermoneutral value reported in literature [45]. Afterwards, the voltage increases as function of current density mainly due to the resistance in the anodic compartment of the cell. Impedance characterizations performed simultaneously on the MEAs allowed to determine the resistance contribution in the polarization curves. The correction of the ohmic drop from the *U–j* plots was done as follows:

$$U_{corr} = U_{app} - IR \quad (3)$$

where U_{corr} (V) is the corrected cell voltage, U_{app} (V) is the applied cell voltage, I (mA) is the measured current density and R, the ohmic resistance (ohm). Resistance values of 110, 102 and 96 mΩ were measured for the catalysts IrO_2, $Ru_{0.8}Ir_{0.2}O_2$ and $Ru_{0.7}Ir_{0.3}O_2$, respectively. This ohmic correction involves *U–j* shapes that provide relevant profiles for water electrolysis process with a voltage close to 1.8 V at 1 A cm^{-2}. The experiments repeated several times under working conditions at 25 °C showed good stability of the synthesized Ru based catalysts in respect of anodic dissolution due undoubtedly to the Ir content as reported by Baglio et al. [36].

4. Conclusion

Ruthenium and iridium based catalysts were synthesized by the thermal decomposition process and investigated as anodes in a proton exchange membrane water electrolysis cell. Physicochemical measurements have shown the presence of the two metals mainly in their oxides form, which permit the activation of the H_2O molecule with low overpotential values. Although ruthenium and iridium remain expensive metal, their utilization in PEM electrolyzers has the advantage to split water at lower potentials than Pt-based catalysts. Moreover, the concomitant presence of IrO_2 and RuO_2 allows to stabilize the catalyst from dissolution, contributing thus to its service life. Nevertheless, the metal oxides have still a non negligible resistance which could be decreased during the preparation in order to enhance the Faradaic efficiency of new generation of electrolyzers for clean hydrogen and oxygen production.

Acknowledgment

The authors gratefully acknowledge financial support from the French National Research Agency ANR-Airelles.

References

[1] C.-J. Winter, Int. J. Hydrogen Energy 34 (2009) S1–S52.
[2] J.F. McElroy, J. Power Sources 47 (1994) 369–375.
[3] J.F. McElroy, J. Power Sources 36 (1991) 219–233.
[4] R. Baldwin, M. Pham, A. Leonida, J. McElroy, T. Nalette, J. Power Sources 29 (1990) 399–412.
[5] H.B. Beer, Improvements in or relating to electrodes for electrolysis, British, 1969.
[6] A.T. Marshall, S. Sunde, M. Tsypkin, R. Tunold, Int. J. Hydrogen Energy 32 (2007) 2320–2324.
[7] A. Marshall, B. Børresen, G. Hagen, M. Tsypkin, R. Tunold, Energy 32 (2007) 431–436.
[8] A. Marshall, B. Børresen, G. Hagen, M. Tsypkin, R. Tunold, Electrochim. Acta 51 (2006) 3161–3167.
[9] A. Marshall, B. Børresen, G. Hagen, M. Tsypkin, R. Tunold, Mater. Chem. Phys. 94 (2005) 226–232.
[10] P. Millet, D. Dragoe, S. Grigoriev, V. Fateev, C. Etievant, Int. J. Hydrogen Energy 34 (2009) 4974–4982.
[11] S.A. Grigoriev, P. Millet, S.A. Volobuev, V.N. Fateev, Int. J. Hydrogen Energy 34 (2009) 4968–4973.
[12] S.A. Grigoriev, P. Millet, S.V. Korobtsev, V.I. Porembskiy, M. Pepic, C. Etievant, C. Puyenchet, V.N. Fateev, Int. J. Hydrogen Energy 34 (2009) 5986–5991.
[13] G. Doucet, C. Etiévant, C. Puyenchet, S. Grigoriev, P. Millet, Int. J. Hydrogen Energy 34 (2009) 4983–4989.
[14] S.A. Grigoriev, P. Millet, V.N. Fateev, J. Power Sources 177 (2008) 281–285.
[15] F.L.S. Purgato, P. Olivi, J.M. Léger, A.R. de Andrade, G. Tremiliosi-Filho, E.R. Gonzalez, C. Lamy, K.B. Kokoh, J. Electroanal. Chem. 628 (2009) 81–89.
[16] J. Ribeiro, D. dos Anjos, J. Léger, F. Hahn, P. Olivi, A. de Andrade, G. Tremiliosi-Filho, K. Kokoh, J. Appl. Electrochem. 38 (2008) 653–662.
[17] F.C. Simões, D.M. dos Anjos, F. Vigier, J.M. Léger, F. Hahn, C. Coutanceau, E.R. Gonzalez, G. Tremiliosi-Filho, A.R. de Andrade, P. Olivi, K.B. Kokoh, J. Power Sources 167 (2007) 1–10.
[18] J. Ribeiro, D.M. dos Anjos, K.B. Kokoh, C. Coutanceau, J.M. Léger, P. Olivi, A.R. de Andrade, G. Tremiliosi-Filho, Electrochim. Acta 52 (2007) 6997–7006.
[19] L.P.R. Profeti, F.C. Simões, P. Olivi, K.B. Kokoh, C. Coutanceau, J.M. Léger, C. Lamy, J. Power Sources 158 (2006) 1195–1201.
[20] J.C. Forti, P. Olivi, A.R. de Andrade, J. Electrochem. Soc. 150 (2003) E222–E226.
[21] L. Ouattara, S. Fierro, O. Frey, M. Koudelka, C. Comninellis, J. Appl. Electrochem. 39 (2009) 1361–1367.
[22] C.P. De Pauli, S. Trasatti, J. Electroanal. Chem. 396 (1995) 161–168.
[23] V.A. Alves, L.A. da Silva, J.F.C. Boodts, S. Trasatti, Electrochim. Acta 39 (1994) 1585–1589.
[24] S. Ardizzone, G. Fregonara, S. Trasatti, Electrochim. Acta 35 (1990) 263–267.
[25] S. Trasatti, Electrochim. Acta 29 (1984) 1503–1512.
[26] J. Rossmeisl, Z.W. Qu, H. Zhu, G.J. Kroes, J.K. Nørskov, J. Electroanal. Chem. 607 (2007) 83–89.
[27] L. Ma, S. Sui, Y. Zhai, Int. J. Hydrogen Energy 34 (2009) 678–684.
[28] C.C. Chang, T.C. Wen, J. Appl. Electrochem. 27 (1997) 355–363.
[29] R. Kötz, S. Stucki, Electrochim. Acta 31 (1986) 1311–1316.
[30] R. Kötz, Electrochim. Acta 29 (1984) 1607–1612.
[31] R. Kötz, H.J. Lewerenz, P. Brüesch, S. Stucki, J. Electroanal. Chem. Interfacial Electrochem. 150 (1983) 209–216.
[32] H. Tamura, C. Iwakura, Int. J. Hydrogen Energy 7 (1982) 857–865.
[33] J.H. Han, S.W. Lee, S.K. Kim, S. Han, C.S. Hwang, C. Dussarrat, J. Gatineau, Chem. Mater. 22 (2010) 5700–5706.
[34] N. Alonso-Vante, I.V. Malakhov, S.G. Nikitenko, E.R. Savinova, D.I. Kochubey, Electrochim. Acta 47 (2002) 3807–3814.
[35] F.I. Mattos-Costa, P. de Lima-Neto, S.A.S. Machado, L.A. Avaca, Electrochim. Acta 44 (1998) 1515–1523.
[36] V. Baglio, A. Di Blasi, T. Denaro, V. Antonucci, A.S. Aricò, R. Ornelas, F. Matteucci, G. Alonso, L. Morales, G. Orozco, L.G. Arriaga, J. New Mater. Electrochem. Syst. 11 (2008) 105–108.
[37] C. Coutanceau, S. Brimaud, C. Lamy, J.M. Léger, L. Dubau, S. Rousseau, F. Vigier, Electrochim. Acta 53 (2008) 6865–6880.
[38] J. Bard Allen, P. Roger, J. Joseph, Standard potentials in aqueous solution, in: A.J. Bard, R. Parsons, J. Jordan (Eds.), Monographs in Electroanalytical Chemistry and Electrochemistry, Dekker Marcel, Inc., New York–Basel, 1985.
[39] A. Manzo-Robledo, A.C. Boucher, E. Pastor, N. Alonso-Vante, Fuel Cells 2 (2002) 109–116.
[40] P.M. Pechini, N. Adams, 3 330 697 ed., United States, 1967.
[41] A.L. Santos, D. Profeti, P. Olivi, Electrochim. Acta 50 (2005) 2615–2621.
[42] Z. Yi, C. Kangning, W. Wei, J. Wang, S. Lee, Ceram. Int. 33 (2007) 1087–1091.
[43] R. Tolba, M. Tian, J. Wen, Z.-H. Jiang, A. Chen, J. Electroanal. Chem. 649 (2010) 9–15.
[44] S. Siracusano, A. Di Blasi, V. Baglio, G. Brunaccini, N. Briguglio, A. Stassi, R. Ornelas, E. Trifoni, V. Antonucci, A.S. Aricò, Int. J. Hydrogen Energy 36 (2011) 3333–3339.
[45] P. Millet, Techniques de l'Ingénieur J4810 (2007) 1–7.